Luminogens

International Edition: DOI: 10.1002/anie.201506782
German Edition: DOI: 10.1002/ange.201506782

Unusual Aggregation-Induced Emission of a Coumarin Derivative as a Result of the Restriction of an Intramolecular Twisting Motion

Fan Bu, Ruihong Duan, Yujun Xie, Yuanping Yi, Qian Peng, Rongrong Hu, Anjun Qin, Zujin Zhao,* and Ben Zhong Tang**

Abstract: *Aggregation-induced emission (AIE) is commonly observed for propeller-like luminogens with aromatic rotors and stators. Herein, we report that a coumarin derivative containing a seven-membered aliphatic ring (CD-7) but no rotors showed typical AIE characteristics, whereas its analogue with a five-membered aliphatic ring (CD-5) exhibited an opposite aggregation-caused quenching (ACQ) effect. Experimental and theoretical results revealed that a large aliphatic ring in CD-7 weakens structural rigidity and promotes out-of-plane twisting of the molecular backbone to drastically accelerate nonradiative excited-state decay, thus resulting in poor emission in solution. The restriction of twisting motion in aggregates blocks the nonradiative decay channels and enables CD-7 to fluoresce strongly. The results also show that AIE is a general phenomenon and not peculiar to propeller-like molecules. The AIE and ACQ effects can be switched readily by the modulation of molecular rigidity.*

The tuning of luminescence on the basis of intramolecular motion has been selected more than once during biological evolution. Many famous biochromophores, for example, green fluorescent protein (GFP)[1–5] and bacterial luciferase (BL),[6–10] testify to the success of this strategy. Experimental and computational investigations show that rotational motion and out-of-plane twisting deformation act as major nonradiative deactivation pathways and efficiently quench the emission of free GFPs and BLs, respectively. When the GFPs are bound in a protein cavity, these intramolecular motions are restricted, and thus, the emission is turned on. In contrast, artificial luminogens are designed preferentially with well-conjugated and planar structures, which facilitate the radiative decay and discourage the nonradiative decay of the excited state. Although the generated luminogens show good emission in solution, emission quenching in aggregates is often observed.[11,12] This aggregation-caused quenching (ACQ) prevents the real-world application of a variety of efficient luminogens, but attempts to solve this thorny problem by molecular engineering and physical technology are usually associated with a high cost and limited success.[13,14]

A series of propeller-like luminogens, such as tetraphenylethenes,[15,16] siloles,[17,18] and phosphindoles,[19,20] show faint emission in the solution state but are tuned to be highly emissive in the aggregated state, thus presenting an interesting phenomenon of aggregation-induced emission (AIE). The working mechanism of the AIE phenomenon is very similar to that for GFP; that is, the rotation of peripheral aromatic rings mainly consumes the excited-state energy in solution, whereas the restriction of intramolecular rotation in aggregates leads to conversion of the energy into photons.[21–27] The structure of most AIE luminogens features several rotors attached to a stator through single bonds, and current designs of AIE luminogens generally comply with this principle. Although this approach enables the straightforward preparation of AIE luminogens, in a sense it kills imagination and constrains the diversity of AIE luminogens. Hence, many π-conjugated planar traditional chromophores are rarely considered to be AIE-active, owing to the lack of aromatic rotors, and there are only limited reports on new hypotheses for unusual AIE systems, such as the restriction of intramolecular charge transfer for electron-donor–acceptor molecules, and the formation of ion pairs for the berberine palmitate dye.[28–30]

Coumarin (chromen-2-one) is a natural organic substance that is abundant in many plants. In the past few decades, structurally diverse coumarin derivatives have been developed and have become a class of dyes of intense interest owing to their wide range of applications in organic lasers, organic light-emitting diodes, fluorescent sensors, and other devices.[31,32] Coumarin derivatives often show very high fluorescence efficiencies of up to unity in the solution state,[33,34] but their planar coumarin skeletons are prone to form strong π–π stacking interactions in the aggregated state. These interactions in many cases quench fluorescence greatly, and undermine the performance of optoelectronic devices.[35,36] Thus, the exploration of facile ways to solve the ACQ problem of coumarin dyes is of high importance for fundamental understanding and real-world utilization. In this study, we investigated the optical properties of two π-expanded coumarin derivatives with very similar structures

[*] F. Bu, Dr. R. Hu, Prof. A. Qin, Prof. Z. Zhao, Prof. B. Z. Tang
State Key Laboratory of Luminescent Materials and Devices
South China University of Technology
Guangzhou 510640 (China)
E-mail: mszjzhao@scut.edu.cn
R. Duan, Y. Xie, Dr. Y. Yi, Dr. Q. Peng
Key Laboratory of Organic Solids
Beijing National Laboratory for Molecular Science
Institute of Chemistry, Chinese Academy of Sciences
Beijing 100190 (China)
E-mail: qpeng@iccas.ac.cn
Prof. B. Z. Tang
Department of Chemistry
The Hong Kong University of Science and Technology
Clear Water Bay, Kowloon, Hong Kong (China)
E-mail: tangbenz@ust.hk

Supporting information for this article is available on the WWW under http://dx.doi.org/10.1002/anie.201506782.

by using complementary spectroscopic and computational methods. The emission behavior of the coumarin derivatives, the structures of which differed only in the size of a fused aliphatic ring, was sensitive to the size of this aliphatic ring (Scheme 1). The molecule with a flexible seven-membered

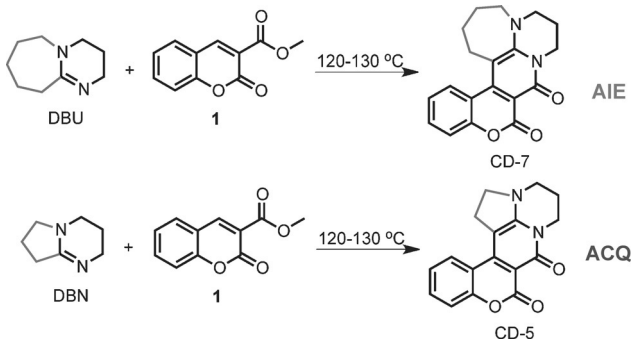

Scheme 1. Synthesis of CD-7 and CD-5.

ring (CD-7) showed typical AIE effect, in complete contrast to the ACQ effect observed for the other molecule with a five-membered ring (CD-5). Our theoretical results showed that the restriction of intramolecular twisting motions is responsible for the unusual AIE activity of coumarin derivative CD-7 without any aromatic rotors.

Two coumarin derivatives, CD-7 and CD-5, were readily prepared in good yield by heating methyl 2-oxo-2*H*-chromene-3-carboxylate (**1**) with DBU and DBN, respectively, at 120 °C for 2 h, according to the method reported by Poronik and Gryko.[37] The absorption properties of CD-7 and CD-5 are similar, with absorption maxima at approximately 412 nm, owing to the identical extent of conjugation. However, the absorption spectrum of CD-7 in CH_2Cl_2 is structureless, whereas that of CD-5 displays doublet fine structure, thus implying that CD-5 has higher structural rigidity than CD-7 (Figure 1 A).

The emission properties of CD-7 differ greatly from those of CD-5 (Figure 1 B). Upon photoexcitation, CD-7 showed faint fluorescence, peaking at 494 nm in CH_2Cl_2, with a quite low absolute fluorescence quantum yield (Φ_F) of 0.5%, whereas CD-5 showed intense blue emission at 443 nm with a Φ_F value as high as 69%. The Stokes shift between the absorption and emission spectra of CD-7 was 82 nm, which is about 2.5 times larger than that of CD-5 (32 nm), thus suggesting that the geometrical modification of CD-7 between the excited and ground states is much larger than that of CD-5. However, the emission behavior of CD-7 and CD-5 as powder samples was exactly opposite to that in CH_2Cl_2. The emission maximum of CD-7 was hypsochromically shifted to 480 nm, with an enhanced Φ_F value of 43% and a far smaller Stokes shift of 68 nm, whereas that of CD-5 was bathochromically shifted to 520 nm, with a greatly decreased Φ_F value of 5.1% and an increased Stokes shift of 109 nm (see Figure S1 in the Supporting Information). Thus, CD-7 exhibited typical AIE characteristics with an AIE factor (the ratio of Φ_F in the powder to that in solution) of 83, but CD-5 showed an apparent ACQ effect.

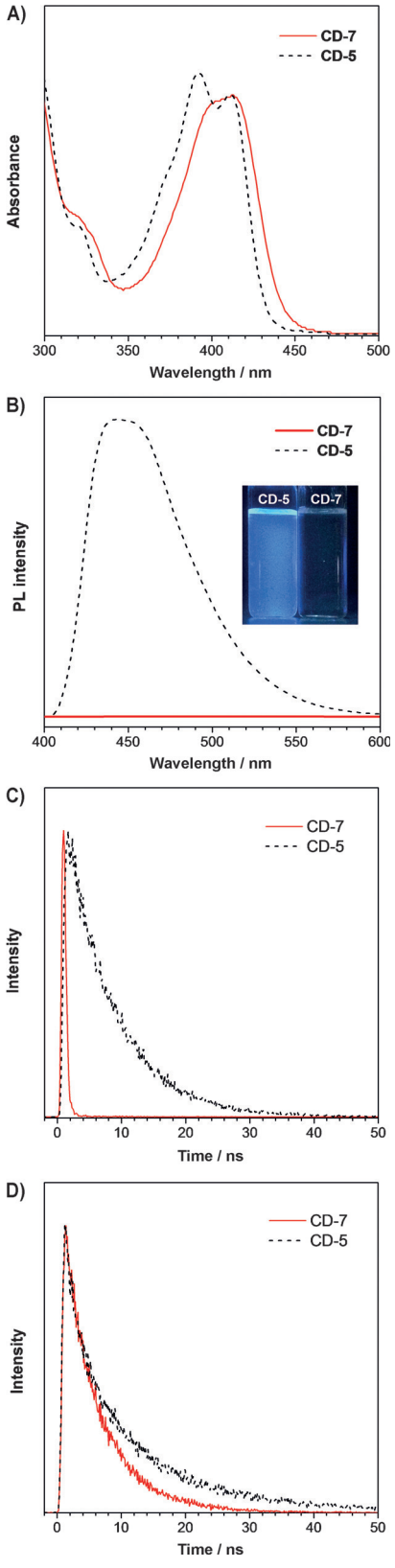

Figure 1. A) Absorption and B) photoluminescence (PL) spectra of CD-7 and CD-5 in CH_2Cl_2. Concentration: 10 μM; excitation wavelength: 411 nm. C,D) Fluorescence decay of CD-7 and CD-5 in CH_2Cl_2 (C) and in the powder (D).

Time-resolved fluorescence spectra (Figure 1 C,D) revealed that the fluorescence lifetime of CD-7 in CH_2Cl_2 was 0.3 ns, which is much shorter than that of CD-5 (7.5 ns). In powder samples, the fluorescence lifetime of CD-7 increased to 5.7 ns, and was thus close to that of CD-5 in solution (in powder samples, CD-5 had a fluorescence lifetime of 10.8). We also estimated the radiative and nonradiative decay rates of CD-7 and CD-5 (Table 1). In CH_2Cl_2, the nonradiative decay rate (ca. $3.0\times10^9\ s^{-1}$) of CD-7 was remarkably larger than the radiative decay rate ($1.6\times10^7\ s^{-1}$) by two orders of magnitude. However, in powder samples, the nonradiative decay rate of CD-7 decreased drastically to $1.0\times10^8\ s^{-1}$, which is close to the radiative rate ($7.5\times10^7\ s^{-1}$). These results suggest that nonradiative decay is dominant for CD-7 in solution, but is weakened to the same level as radiative decay in powder samples. The radiative decay rate of CD-5 was significantly lower in powder samples than in solution, thus implying that nonradiative decay becomes a major pathway in powder samples.

Table 1: Optical properties of CD-7 and CD-5.

	λ_{abs} [nm] CH_2Cl_2	λ_{em} [nm] (Φ_F [%])[a] CH_2Cl_2	powder	τ [ns] (k_r [$10^7\ s^{-1}$], k_{nr} [$10^7\ s^{-1}$])[b] CH_2Cl_2	powder
CD-7	412	494 (0.5)	480 (43)	0.3 (1.6, 301.5)	5.7 (7.5, 10.0)
CD-5	411	443 (69)	520 (5.1)	7.5 (9.4, 4.0)	10.8 (0.6, 8.7)

[a] The fluorescence quantum yields were measured with an absolute fluorescence quantum yield spectrometer. [b] Rate constants for radiative (k_r) and nonradiative decay (k_{nr}) were calculated from the Φ_F and τ values according to the formulae $k_r=\Phi_F/\tau$ and $k_{nr}=(1-\Phi_F)/\tau$.

To better understand the solid-state photophysical properties, we scrutinized the packing model of CD-7 in the crystalline state (Figure 2).[37] The CD-7 molecules adopt a slightly twisted conformation, and the seven-membered aliphatic ring lies out of the plane of the conjugated molecular backbone. The molecules are arranged in a loose manner, and π–π intermolecular interactions are hampered among CD-7 molecules, owing to steric hindrance imposed by the seven-membered aliphatic ring. Multiple C–H···O hydrogen bonds with distances in the range of 2.5–2.8 Å are formed between the aliphatic ring and the carbonyl groups of adjacent molecules . The collective force of these weak electrostatic interactions can rigidify the molecular conformation of CD-7 in the solid phase without causing excimer and large excitonic interactions among molecules. The crystal of CD-5 is not available, but it is reasonable to suppose a tighter and closer packing because of its more planar conformation. The induced π–π stacking interaction can severely weaken emission intensity and move the emission spectrum into the long-wavelength region.

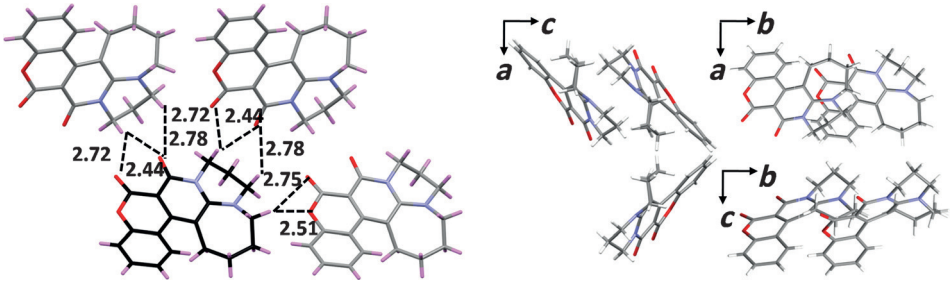

Figure 2. A) C–H···O hydrogen bonds in the crystal of CD-7 (labeled in Å). B) Molecular packing of CD-7.

To further decipher the optical properties of CD-7 and CD-5, we studied their electronic structures theoretically in the ground state (S_0) and the excited state (S_1) at the level of (TD) M062X/6-31G*. The HOMO and LUMO orbitals and energy levels are plotted in Figure 3 for CD-7 and CD-5 with S_0 geometry. The frontier orbitals of CD-7 and CD-5 are indicative of a π–π* transition with a degree of charge-transfer character. The electron density of CD-7 and CD-5 is mainly distributed over the conjugated framework (chromeno[3,4-*c*]pyridine-4,5(3*H*)-dione) and the neighboring alkyl groups, whereas the additional two methylene groups in CD-7 show nearly no contribution. The similarity in the electronic structures of CD-7 and CD-5 in the S_0 state is consistent with the absorption spectra, but fails to explain their opposite emission behavior. Therefore, we focus on the difference in the geometric structures of CD-7 in the S_0 and S_1 states in the gas phase and in aggregates.

We considered the aggregation effect by computing the geometric and electronic structures of a large enough cluster cut from the crystal structure by using a combined quantum-mechanics and molecular-mechanics (QM/MM) approach (see Figure S2 for the QM/MM model).[38,39] The S_0 geometries of CD-7 in the gas and solid phases are almost the same (Figure 4), except for a minor difference in the degree of torsion of the seven-membered aliphatic ring and the pyridinone fragment away from the chromen-2-one mean plane. The S_1 geometry of CD-7 in the gas phase is very different to the S_0 geometry. A large alteration of about 18° in the mean torsion angle between the pyridinone and chromen-2-one fragments (see Table S1 in the Supporting Information) was found in the $S_0\rightarrow S_1$ transition process, thus revealing that the molecule undergoes out-of-plane twisting motions along the C2–C7 bond under photoexcitation. In the solid phase, the geometrical modification of CD-7 is smaller (ca. 5°), which suggests that the intramolecular twisting motion is restricted to a large extent. In sharp contrast, CD-5 has a more planar conformation of the conjugated framework in both the S_0 and S_1 states, and experiences little variation upon photoexcitation even in the gas phase, thus demonstrating its intrinsic structural rigidity. Owing to the lack of a crystal structure, the construction and optimization of the molecular

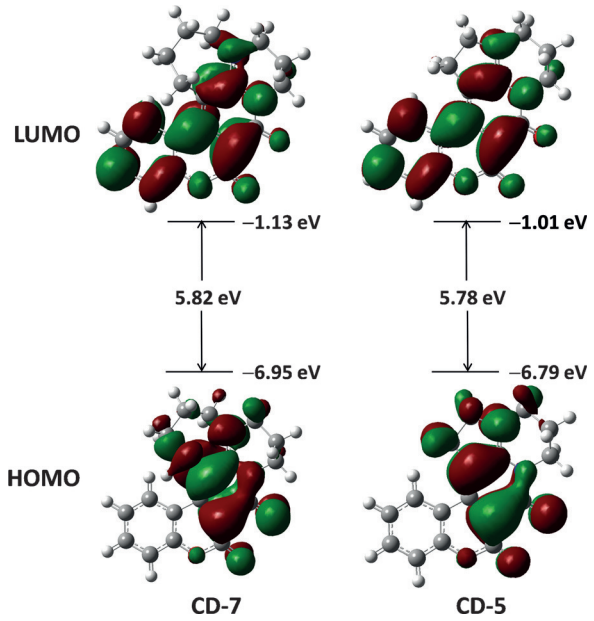

Figure 3. Molecular-orbital amplitude plots and energy levels of the HOMOs and LUMOs of CD-7 and CD-5, as calculated at the level of M062X/6-31G*.

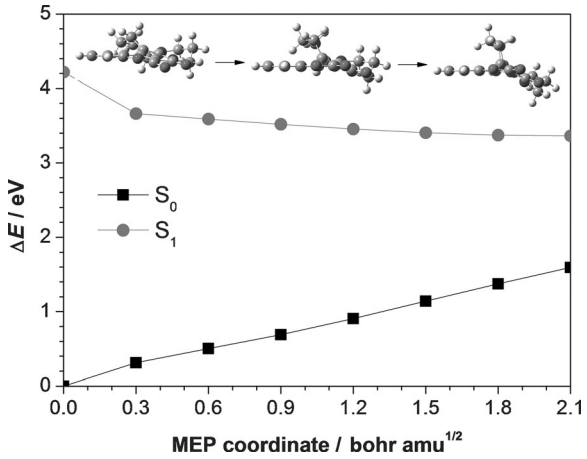

Figure 5. Energy profiles of the S_0 and S_1 states along the S_1-state minimum-energy path (MEP) at the CASSCF level.

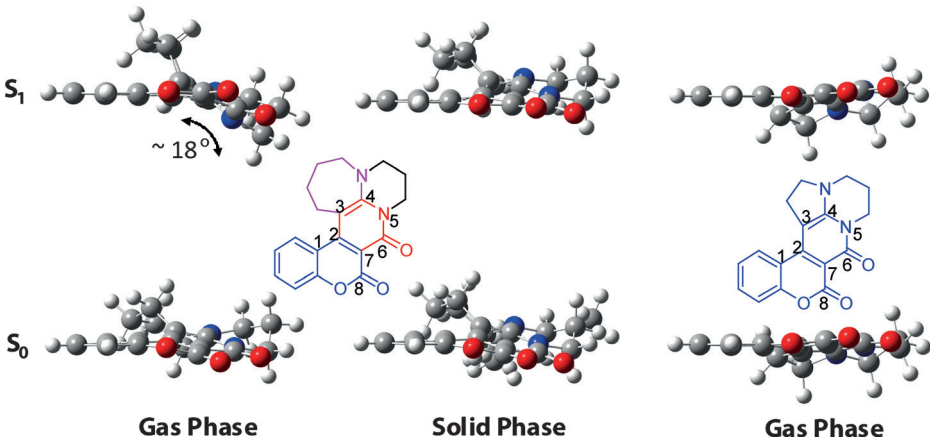

Figure 4. Optimized S_0 and S_1 geometric structures of CD-7 in the gas and solid phases and CD-5 in the gas phase.

packing of CD-5 in the solid phase are technically difficult, and are not discussed herein.

To gain deeper insight into the deactivation mechanism of the excited state, we found the minimum-energy path (MEP; Figure 5) on the S_1 potential-energy surface of CD-7, which starts at the S_0 geometry and ends at the S_1 geometry, by using the more accurate CASSCF method (see Figure S3). Along the MEP coordinate, the energy gap between the S_1 and S_0 states gradually decreases, until it finally reaches the minimum value of 1.77 eV at the S_1 geometry. It is clear that no intersection crossing in the Franck–Condon region appears, in good agreement with the experimental nonradiative decay time of the order of nanoseconds, which is far slower than the typical ultrafast process induced by intersection crossing, with decay times of the order of femtoseconds.[40] Therefore, the activated intramolecular twisting motions are responsible for the nonradiative internal conversion (IC) of CD-7 in solution. The contribution of intersystem crossing was not considered, as the phosphorescence was not observed at low temperature, and the spin–orbit coupling between the S_1 and T_1 states is 0.4 cm^{-1} for CD-7, as calculated by using the BDF package.[41] This value is remarkably smaller than the non-adiabatic electronic coupling for typical internal-conversion processes in organic molecules (from about a few tens to hundreds and even thousands of reciprocal centimeters).[42] In the aggregated state, the intermolecular interactions between molecules restrict the intramolecular twisting motions and largely block the nonradiative internal conversion. Consequently, the excited-state energy is mostly transformed into photons, and strong emission is observed.

The optical behavior of CD-7 is completely identical to that of typical AIE molecules. The absorption maximum of CD-7 hardly varies from solution to the aggregate, whereas its emission peak is strongly blue-shifted. This effect should be mainly caused by the significant decrease in the molecular-reorganization energy (from 4028 cm^{-1} in solution to 3438 cm^{-1} in aggregates), owing to the restriction of twisting motion in aggregates.[43] The AIE mechanism can be understood readily in view of the change in the character of the potential-energy surface of low-frequency twisting modes from solution to the solid (Figure 6). In solution, the potential-energy surface of the S_1 state is very flat, and many vibrational states with high quanta numbers are involved. These vibrational states overlap well with the vibrational states of the S_0 state and sharply accelerate the rate of internal conversion. In contrast, in the solid, the

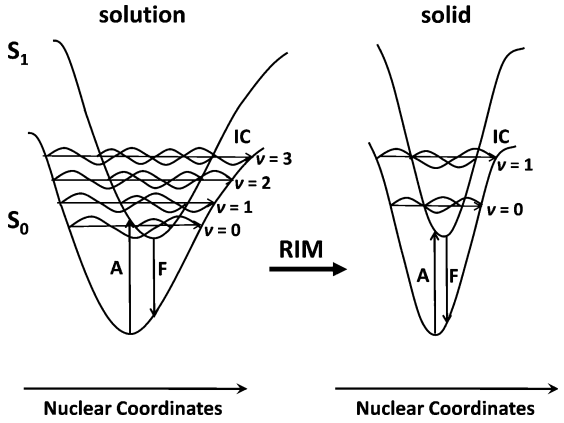

Figure 6. Sketch of the potential-energy surfaces of low-frequency twisting modes for CD-7 in solution and in the solid phase (RIM = restriction of intramolecular motion).

twisting motion is hampered by the steric constraints and interactions from the surrounding molecules, and higher energies are needed, which results in a steep potential-energy surface. In this case, there are few vibrational states, and the overlap of the wavefuntions of the S_0 and S_1 states becomes less effective. Therefore, the nonradiative decay channels are blocked, and the emission is turned on.

Because of the contrasting emission behavior of CD-7 and CD-5, it is reasonable that the out-of-plane twisting motion of the pyridinone fragment relative to the chromen-2-one moiety correlates closely with the nonradiative excited-state decay and accounts for the faint and red-shifted emission of CD-7 in solution. In the solid, the intramolecular motion is restricted, and the radiative excited-state decay becomes dominant, thus enabling the molecule to fluoresce strongly. Meanwhile, the steric hindrance from the seven-membered aliphatic ring hampers the close π–π stacking of the molecules and alleviates emission quenching. In the counterpart CD-5 with a smaller ring size, the structural planarity and rigidity are improved, which reduces the nonradiative decay and affords good emission efficiency in solution. However, owing to its planar conformation, CD-5 experiences strong π–π intermolecular interactions and suffers severe emission quenching in the solid, thus leading to greatly decreased emission efficiency and a red-shifted emission spectrum. In this case, it possible to switch between the AIE and ACQ effects by simply altering the size of the electronically independent aliphatic ring, without impacting the electronic nature of the conjugated framework.

In summary, we investigated the optical properties of two readily prepared coumarin derivatives, CD-7 and CD-5, and found that although their molecular structures are similar, they exhibit opposite emission behavior. Whereas CD-5 shows an ACQ effect, CD-7 exhibits intriguing AIE characteristics, which originate from its intrinsic structural flexibility and nonplanarity. The restriction of intramolecular twisting motions is thought to be the underlying mechanism for the unusual AIE effect. The size of the aliphatic ring plays a key role in modulating the molecular rigidity and controlling the intramolecular twisting motions and intermolecular interactions. Importantly, CD-7 is an unconventional aromatic rotor-free AIE luminogen derived from a natural substance. It differs greatly from common propeller-like AIE luminogens containing aromatic rotors, and may inspire a novel coumarin-based AIE system with the merits of natural origin, structural diversity, and great potential in biotechnology and materials science. Our results also reveal that the AIE phenomenon is not peculiar to specific molecules and provide an approach to the creation of AIE luminogens from common dyes by controlling intramolecular motions. We believe this mechanistic elucidation is helpful to eliminate the structural limits of AIE and ACQ dyes, both of which can be readily transformed by the modulation of molecular rigidity.

Experimental Section

Materials and instruments: UV/Vis absorption spectra were recorded on a Shimadzu UV-2600 spectrophotometer. Photoluminescence spectra were recorded on a Horiba Fluoromax-4 spectrofluorometer. Fluorescence quantum yields were determined with a Hamamatsu C11347 Quantaurus-QY absolute fluorescence quantum yield spectrometer. Fluorescence lifetimes were determined with a Hamamatsu C11367-11 Quantaurus-Tau time-resolved spectrometer. Spectrophotometric-grade solvents were used in the measurements without further purification.

Ab initio calculations: The equilibrium geometries were determined at the DFT/TD-DFT level. No symmetry constraint was adopted for either gas- or solid-phase optimizations. The M062X functional and 6-31G* basis set were used. The analytical frequencies of S_0 at the DFT level and numerical frequencies of S_1 at the TD-DFT level were evaluated to ensure the absence of imaginary frequencies in the gas phase. The QM/MM calculations were carried out by the two-layer ONIOM method with the central molecule as the high-layer QM part and the surrounding molecules as the low-layer MM part. The QM/MM model was constructed by cutting a large enough cluster from the crystal structure (see Figure S2). All calculations were performed by using the D.01 version of the Gaussian 09 package.

CASSCF computational protocol: The MEP calculation for CD-7 was performed at the two-root state-averaged CASSCF level of theory with a 6-31G* basis set. The CASSCF wave function comprised an active space of 8 electrons in 8 orbitals (see Figure S1 for a full description of the active space), and comprised π and π* orbitals involved in the π-conjugated system of CD-7. The full active space (including all π and π* orbitals) would comprise 18 electrons and 15 orbitals, but in this study we used a slightly reduced active space of 8 electrons and 8 orbitals; thus, 7 orbitals and 10 electrons were excluded from the active space owing to the high computational cost of using the full active space. The n orbitals were excluded from the active space, since the n,π* states are assumed to be high in energy on the basis of earlier TD-DFT studies. As the internal-conversion process investigated in this study does not involve bond breaking or electronic excitation of the σ framework, we did not include the corresponding σ orbitals in the active space. The MEP calculation was performed with Molcas v.8.0. It was computed in the form of an intrinsic reaction coordinate, with a step constraint of 0.3 Bohr amu$^{1/2}$. The starting Franck–Condon point was the S_0 geometry obtained by B3lyp/6-31G*.

Acknowledgements

We acknowledge financial support from the National Natural Science Foundation of China (51273053), the National Basic Research Program of China (973 Program, 2013CB834702), the Guangdong Natural Science Funds for Distinguished

Young Scholars (2014A030306035), the Guangdong Innovative Research Team Program of China (201101C0105067115), and the Fundamental Research Funds for the Central Universities (2015PT020).

Keywords: aggregation-induced emission · coumarins · density functional calculations · excited-state decay · intramolecular twisting

How to cite: *Angew. Chem. Int. Ed.* **2015**, *54*, 14492 – 14497
Angew. Chem. **2015**, *127*, 14700 – 14705

[1] Y. H. Hsu, Y. A. Chen, H. W. Tseng, Z. Zhang, J. Y. Shen, W. T. Chuang, T. C. Lin, C. S. Lee, W. Y. Hung, B. C. Hong, S. H. Liu, P. T. Chou, *J. Am. Chem. Soc.* **2014**, *136*, 11805 – 11812.
[2] M. E. Martin, F. Negri, M. Olivucci, *J. Am. Chem. Soc.* **2004**, *126*, 5452 – 5464.
[3] K. Y. Chen, Y. M. Cheng, C. H. Lai, C. C. Hsu, M. L. Ho, G. H. Lee, P. T. Chou, *J. Am. Chem. Soc.* **2007**, *129*, 4534 – 4535.
[4] C. C. Hsieh, P. T. Chou, C. W. Shih, W. T. Chuang, M. W. Chung, J. Lee, T. Joo, *J. Am. Chem. Soc.* **2011**, *133*, 2932 – 2943.
[5] W. T. Chuang, C. C. Hsieh, C. H. Lai, C. W. Shih, K. Y. Chen, W. Y. Hung, Y. H. Hsu, P. T. Chou, *J. Org. Chem.* **2011**, *76*, 8189 – 8202.
[6] S. Ghisla, V. Massey, J. M. Lhoste, S. G. Mayhew, *Biochemistry* **1974**, *13*, 589 – 597.
[7] J. Li, Z. Liu, C. Tan, X. Guo, L. Wang, A. Sancar, D. Zhong, *Nature* **2010**, *466*, 887 – 890.
[8] Y. T. Kao, C. Saxena, L. Wang, A. Sancar, D. Zhong, *Proc. Natl. Acad. Sci. USA* **2005**, *102*, 16128 – 16132.
[9] D. Zhou, E. Mirzakulova, R. Khatmullin, I. Schapiro, M. Olivucci, K. D. Glusac, *J. Phys. Chem. B* **2011**, *115*, 7136 – 7143.
[10] S. Gozem, E. Mirzakulova, I. Schapiro, F. Melaccio, K. D. Glusac, M. Olivucci, *Angew. Chem. Int. Ed.* **2014**, *53*, 9870 – 9875; *Angew. Chem.* **2014**, *126*, 10028 – 10033.
[11] J. E. Anthony, *Chem. Rev.* **2006**, *106*, 5028 – 5048.
[12] T. M. Figueira-Duarte, K. Müllen, *Chem. Rev.* **2011**, *111*, 7260 – 7314.
[13] J. A. Rogers, T. Someya, Y. Huang, *Science* **2010**, *327*, 1603 – 1607.
[14] R. A. Miller, E. A. Chandross, *Chem. Rev.* **2010**, *110*, 1 – 574.
[15] Z. Zhao, J. W. Y. Lam, B. Z. Tang, *J. Mater. Chem.* **2012**, *22*, 23726 – 23740.
[16] Z. Zhao, P. Lu, J. W. Y. Lam, Z. Wang, C. Y. K. Chan, H. H. Y. Sung, I. D. Williams, Y. Ma, B. Z. Tang, *Chem. Sci.* **2011**, *2*, 672 – 675.
[17] Z. Zhao, B. He, B. Z. Tang, *Chem. Sci.* **2015**, *6*, 5347 – 5365.
[18] Z. Zhao, Z. Wang, P. Lu, C. Y. K. Chan, D. Liu, J. W. Y. Lam, H. H. Y. Sung, I. D. Williams, Y. Ma, B. Z. Tang, *Angew. Chem. Int. Ed.* **2009**, *48*, 7608 – 7611; *Angew. Chem.* **2009**, *121*, 7744 – 7747.
[19] A. Fukazawa, Y. Ichihashi, S. Yamaguchi, *New J. Chem.* **2010**, *34*, 1537 – 1540.
[20] F. Bu, E. Wang, Q. Peng, R. Hu, A. Qin, Z. Zhao, B. Z. Tang, *Chem. Eur. J.* **2015**, *21*, 4440 – 4449.
[21] S. Yin, Q. Peng, Z. Shuai, W. Fang, Y. H. Wang, Y. Luo, *Phys. Rev. B* **2006**, *73*, 205409.
[22] Q. Peng, Y. Yi, Z. Shuai, J. Shao, *J. Am. Chem. Soc.* **2007**, *129*, 9333 – 9339.
[23] Y. Hong, J. W. Y. Lam, B. Z. Tang, *Chem. Commun.* **2009**, 4332 – 4353.
[24] Y. Hong, J. W. Y. Lam, B. Z. Tang, *Chem. Soc. Rev.* **2011**, *40*, 5361 – 5388.
[25] J. Mei, Y. Hong, J. W. Y. Lam, A. Qin, Y. Tang, B. Z. Tang, *Adv. Mater.* **2014**, *26*, 5429 – 5479.
[26] S. Dong, Z. Li, J. Qin, *J. Phys. Chem. B* **2009**, *113*, 434 – 441.
[27] Q. Zhu, Y. Zhang, H. Nie, Z. Zhao, S. Liu, K. S. Wong, B. Z. Tang, *Chem. Sci.* **2015**, *6*, 4690 – 4697.
[28] T. Nishiuchi, K. Tanaka, Y. Kuwatani, J. Sung, T. Nishinaga, D. Kim, M. Iyoda, *Chem. Eur. J.* **2013**, *19*, 4110.
[29] B.-R. Gao, H.-Y. Wang, Y.-W. Hao, L.-M. Fu, H.-H. Fang, Y. Jiang, L. Wang, Q.-D. Chen, H. Xia, L.-Y. Pan, Y.-G. Ma, H.-B. Sun, *J. Phys. Chem. B* **2010**, *114*, 128 – 134.
[30] J. Chahine, N. Saffon, M. Cantuel, S. Fery-Forgues, *Langmuir* **2011**, *27*, 2844 – 2853.
[31] R. O'Kennedy, R. D. Thornes, *Coumarins: Biology, Applications and Mode of Actions*, Wiley, Chichester, **1997**.
[32] M. Tasior, D. Kim, S. Singha, M. Krzeszewski, K. H. Ahn, D. T. Gryko, *J. Mater. Chem. C* **2015**, *3*, 1421 – 1446.
[33] S. Nad, M. Kumbhakar, H. Pal, *J. Phys. Chem. A* **2003**, *107*, 4808 – 4816.
[34] C.-T. Chen, C.-L. Chiang, Y.-C. Lin, L.-H. Chan, C.-H. Huang, Z.-W. Tsai, C.-T. Chen, *Org. Lett.* **2003**, *5*, 1261 – 1264.
[35] S. Kumar, P. Singh, R. Srivastava, R. R. Koner, A. Pramanik, J. Mathew, S. Sinha, M. Rawat, R. S. Anand, S. Ghosh, *J. Mater. Chem. C* **2014**, *2*, 6637 – 6647.
[36] H. Moon, Q. P. Xuan, D. Kim, Y. Kim, J. W. Park, C. H. Lee, H.-J. Kim, A. Kawamata, S. Y. Park, K. H. Ahn, *Cryst. Growth Des.* **2014**, *14*, 6613 – 6619.
[37] Y. M. Poronik, D. T. Gryko, *Chem. Commun.* **2014**, *50*, 5688 – 5690.
[38] G. Yu, S. Yin, Y. Liu, J. Chen, X. Xu, X. Sun, D. Ma, X. Zhan, Q. Peng, Z. Shuai, B. Z. Tang, D. Zhu, W. Fang, Y. Luo, *J. Am. Chem. Soc.* **2005**, *127*, 6335 – 6346.
[39] T. Zhang, Y. Jiang, Y. Niu, D. Wang, Q. Peng, Z. Shuai, *J. Phys. Chem. A* **2014**, *118*, 9094 – 9104.
[40] W. Domcke, D. R. Yarkony, H. Koppel, *Conical Intersections: Electronic Structure, Dynamics and Spectroscopy*, World Scientific, Singapore, **2004**, pp. 739 – 802.
[41] Z. Li, Y. Xiao, W. Liu, *J. Chem. Phys.* **2012**, *137*, 154114.
[42] S. W. Yin, Q. Peng, Z. Shuai, W. H. Fang, Y. H. Wang, Y. Luo, *Phys. Rev. B* **2006**, *73*, 205409.
[43] Q. Wu, T. Zhang, Q. Peng, D. Wang, Z. Shuai, *Phys. Chem. Chem. Phys.* **2014**, *16*, 5545 – 5552.

Received: July 22, 2015
Revised: August 31, 2015
Published online: October 6, 2015

